J.Natn.Sci.Foundation Sri Lanka 2025 53 (3): 259 - 272
DOI: http://dx.doi.org/10.4038/jnsfsr.v53i3.12624

RESEARCH ARTICLE

Earthquake Engineering

Effect of initial imperfections on the seismic performance of thin-walled steel hollow piers: A numerical approach.

AGYM Kumara, ACD Pigera, NAI Ayodya, JASC Jayasinghe* and CS Bandara
Department of Civil Engineering, Faculty of Engineering, University of Peradeniya, Peradeniya, Sri Lanka.

Submitted: 30 March 2025; Revised: 10 August 2025; Accepted: 27 August 2025

Abstract: This research investigates the influence of initial imperfections on the seismic performance of steel hollow piers, which are crucial components of bridges and other critical structures. The study focuses on two main types of initial imperfections: residual stresses and global geometric imperfections, which are key parameters influencing the seismic performance of thin-walled steel hollow piers. The goal is to understand how these imperfections affect the pier's ductility, maximum energy dissipation capacity, and overall behaviour under uni-directional cyclic loads which simulates the seismic loading conditions. A numerical model was developed using the finite element method (FEM), incorporating various imperfection profiles and tested under different loading directions. Parametric studies were conducted to observe the effects of imperfections within permissible limits, as well as beyond those limits. The results revealed that the residual stresses had a negligible impact on seismic performance. However, global geometric imperfections significantly influenced the performance when the bend exceeded the allowable limit, and loaded in line with the imperfection, which is particularly critical. The study shows that global imperfections lead to a significant reduction in maximum strength, with reductions as high as 24% when loaded in line with the imperfection and between 1% and 11% when loaded perpendicularly, and these findings indicate that global imperfections play a dominant role in failure modes due to lateral cyclic loading.

Keywords: Cyclic loading, FE modelling, geometric imperfections, residual stresses, steel hollow piers.

INTRODUCTION

Steel hollow box piers, constructed from welded steel plates, are widely used as essential lateral and vertical force-resisting elements in structures such as bridges, towers, flyovers, wind turbines, buildings, offshore platforms, elevated storage tanks, and transmission towers due to their compact cross-section and advantages such as high earthquake resistance, strength-to-weight ratio, and torsional stiffness (Kearns *et al.*, 1976; Thevega *et al.*, 2021). However, with global population growth and rapid urbanization, structural damage due to seismic events has become increasingly critical. Earthquakes are among the most destructive natural disasters, causing significant economic losses and casualties. Dense urban populations and critical infrastructure in earthquake-prone areas heighten the risks to vital structures like bridges (Aoki *et al.*, 2005). In Japan, for instance, earthquakes between 1923 and 1983 damaged over 3,000 bridges, emphasizing the need for improved seismic design (Kearns *et al.*, 1976).

Traditional seismic design models primarily consider constant axial loads and uni-directional forces. However, real-world seismic movements are multi-dimensional and highly complex. Research indicates that multi-directional

* Corresponding author (supunj@eng.pdn.ac.lk; https://orcid.org/0000-0003-1054-9358)

cyclic lateral stresses impact thin-walled steel tubular columns more severely than single-directional forces. Global buckling under cyclic loading can significantly reduce the strength and ductility of columns, increasing their susceptibility to failure (Aoki *et al.*, 2005). The most common failure mode in steel columns of highway bridge piers under lateral cyclic loading is excessive lateral deformation caused by local buckling of steel plates (Thevega *et al.*, 2021). Both local and global buckling contribute to strength and ductility reduction, ultimately leading to failure.

Imperfections in fabrication of such structures are an unavoidable circumstance. These imperfections can be mainly categorized into three sections: residual stresses, local geometric imperfections, and global geometric imperfections (Sato *et al.*, 2017). This study focuses on the effects of global imperfections and residual stresses on seismic performance. Early geometric imperfections and residual stresses influence the initial stiffness and strength of thin-walled structures under monotonic loading (Mamaghani *et al.*, 1996; Banno *et al*., 2005). While previous studies, such as those by Jenothan *et al.* (2023), did not account for initial geometric imperfections and residual stresses due to a lack of quantification in tested columns, this study aims to bridge that research gap.

The main focus of this study is to evaluate the seismic performance of thin-walled steel hollow piers by analyzing the effects of initial imperfections, including residual stresses and global geometric imperfections. A finite element (FE) model of the steel pier was developed using ABAQUS software, with validation achieved through comparison with experimental data from Susantha *et al.* (2007). Parametric studies were conducted numerically to assess the influence of residual stresses and geometric imperfections. A selected residual stress distribution from the literature was applied to the model to examine its impact on seismic behaviour. Various curved shape profiles with increasing deflection values were introduced to evaluate global geometric imperfections, as referenced by Sato *et al.* (2017), both within and beyond permissible limits. The study also analyzed how different loading directions influenced the pier's strength and stability.

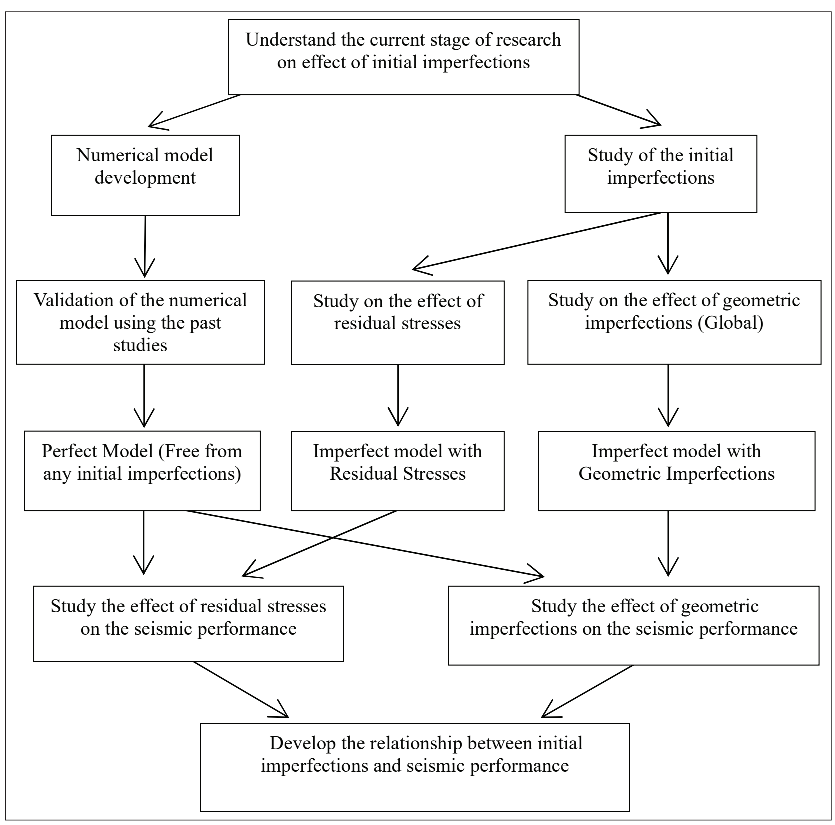

Figure 1: Flow chart of methodology

In addition to these factors, key design parameters such as axial load-to-yield load ratio (P/P_y), width-to-thickness ratio (R_f), and slenderness ratio (λ) were examined in relation to imperfections. The seismic performance was evaluated by analyzing normalized ductility (δ_{max}/δ_y) and maximum strength capacity (H_{max}/ H_y), providing insights into how imperfections affect the pier's response during seismic events.

MATERIALS AND METHODS

Methodology

A research methodology was developed addressing all the research gaps, leading to a parametric study. Following validation of the numerical model, parametric studies were conducted as outlined in the overall methodology diagram shown in Figure 1, which presents a structured approach, beginning with an initial literature review of research on initial imperfections, followed by detailed parametric studies targeting two imperfection types: residual stress (RS) and global geometric imperfections (GI).

Material properties

This study utilizes ABAQUS, a commercial finite element software, to perform FE analysis, incorporating both material and geometric nonlinearities throughout the computation. Accurate material properties are the main factor in obtaining realistic results through numerical simulations. A number of material models for common materials such as steel, concrete and various composites are readily available in ABAQUS. Basic material properties such as yield stress, ultimate stress, Young's modulus, and Poisson's ratio, which determine the behaviour of steel, were introduced to the software. A combined hardening material model is employed, incorporating the Von Mises yield criterion alongside an associated plastic flow rule, effectively modeling the inelastic behaviour of materials under cyclic loading. Normal-strength steel, specifically SM490 (Susantha *et al.*, 2005) grade as per Japanese Industrial Standards, is used in this investigation. The detailed material properties, consistent with those used by Susantha *et al.* (2005), are provided in Table 1. A simplified bilinear material model shown in Figure 2 was used for the analysis for efficient computations without compromising the accuracy of the results.

Table 1: Material properties (Susantha *et al*., 2005)

Parameters	Values
Yield stress (σ_y)	412 MPa
Young's modulus (E_s)	206000 MPa
Ultimate stress (σ_u)	650 MPa
Poisson's ratio (v)	0.276

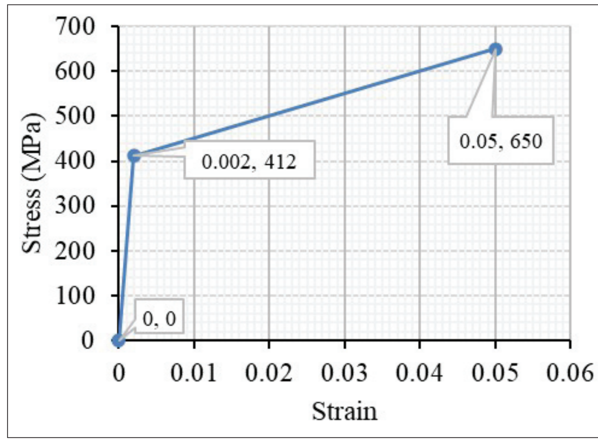

Figure 2: Bilinear stress-strain steel model

Geometric details of columns

Figure 3 displays the longitudinal dimensions of the modeled pier in a 3D view, highlighting cross-sectional and diaphragm dimensions. The same cross-sectional details were applied for validation and the residual stress study, while the parametric analysis for global imperfections included variations in cross-sectional dimensions and pier heights.

Loading procedure

The loading setup in this study starts with an initial axial force to represent the loads coming from the superstructure, denoted as P, followed by the application of unidirectional cyclic lateral loads. The axial force P is represented as a ratio, P/P_y , where P_y refers to the axial force at the yield stress of the steel, in a given cross-section, set to 0.2 in this analysis. A uni-directional cyclic load, which is varying according to the pattern shown in Figure 4 was applied at the top of the model to represent simplified earthquake condition while keeping the constant axial load applied, as shown in Figure 5.

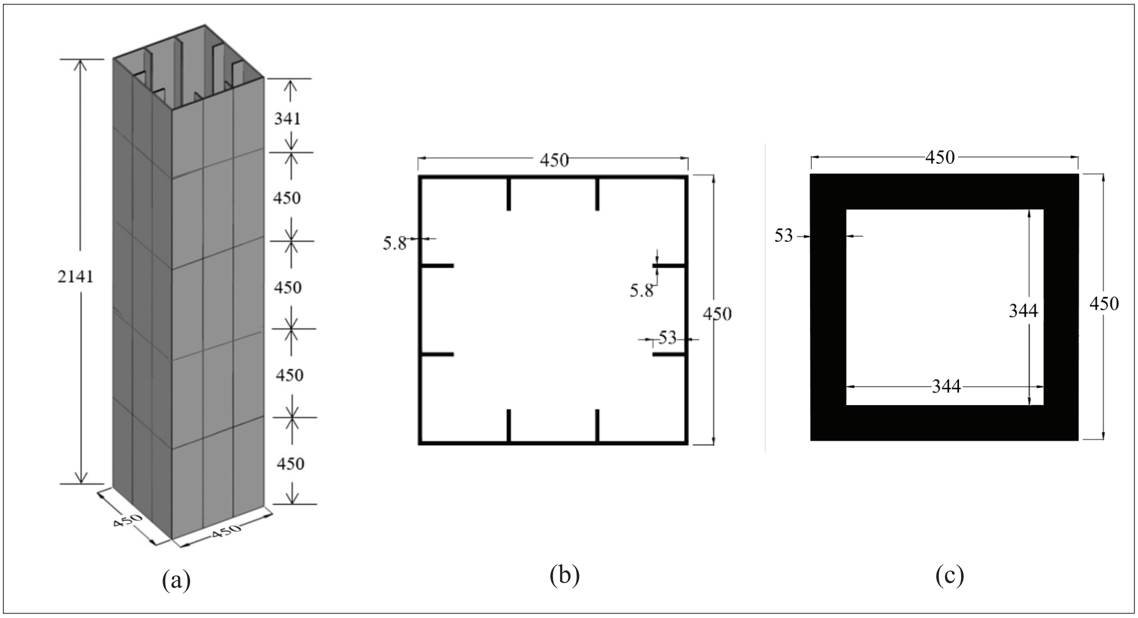

Figure 3: Dimensions of modelled pier: (a) longitudinal, (b) cross-section and (c) intermediate diaphragms (all dimensions are in millimetres)

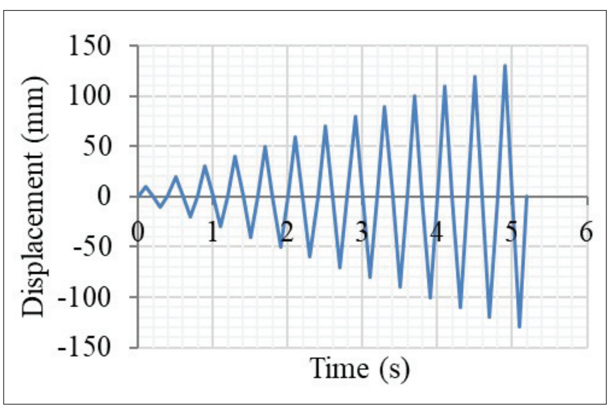

Figure 4: Cyclic loading pattern

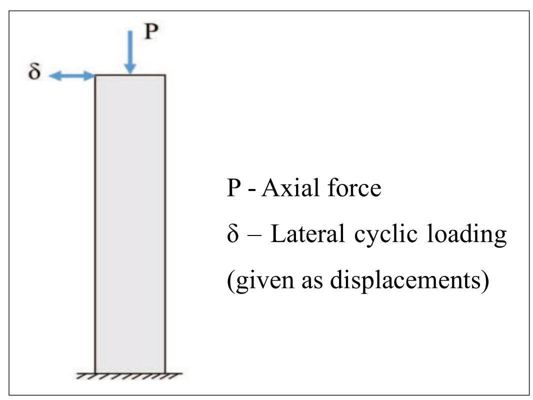

Figure 5: Loading arrangement

A 'perfect model,' which excludes any initial imperfections, was developed in order to compare the performances of the piers in which the initial imperfections were introduced. In this model, the box pier, longitudinal stiffeners, and diaphragms are represented using four-node shell elements with reduced integration (S4R) and five integration points through the thickness. A fixed boundary condition is applied at the base, and axial and lateral cyclic loads are introduced through a reference point linked to the top of the column via a rigid connection. Observations from the previous studies shows that the square box columns made of thin-walled steel indicate that local buckling typically occurs between the base and the bottom diaphragm near the column base. The entire pier is meshed with a 25 mm S4R element size as shown in Figure 6. Mesh convergence testing verified that this mesh density provides accurate results while keeping computational time manageable.

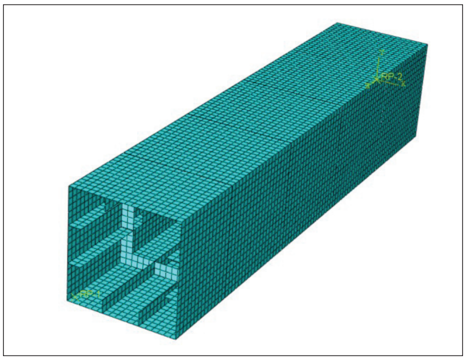

Figure 6: Numerical model of the steel pier

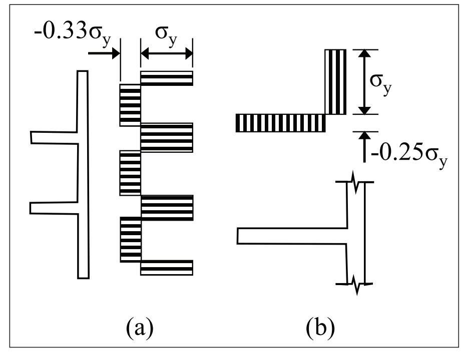

Figure 7: Assumed residual stress distributions: (a) panel and (b) stiffener (Susantha *et al.*, 2005)

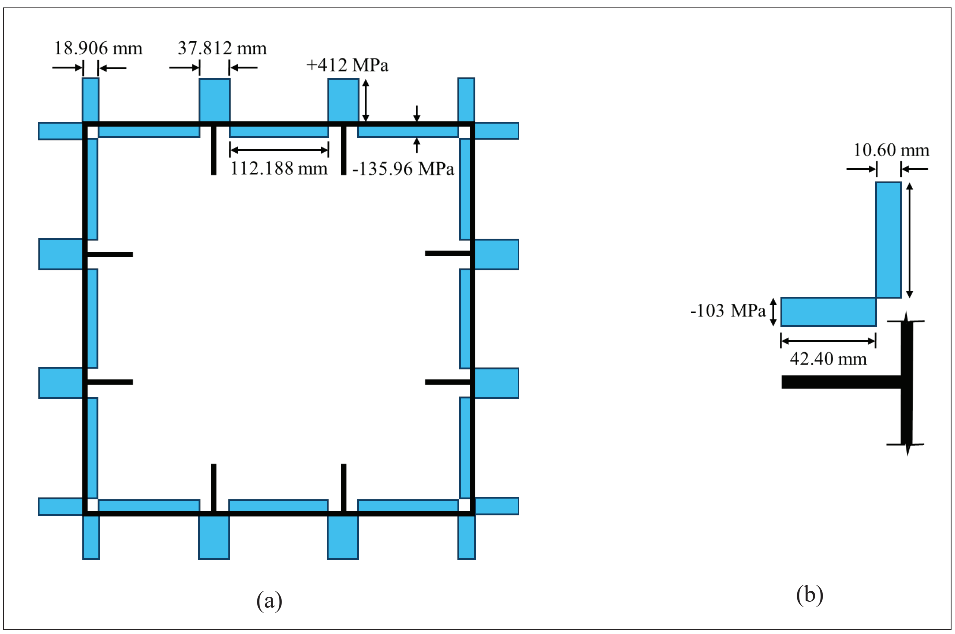

Figure 8: Calculated residual stress distribution values: (a) test pier and (b) stiffener

Numerical model with residual stress

This section evaluates the impact of residual stress on the seismic behaviour of steel piers. The investigation was based on the claim by Jenothan *et al.* (2023a) that neither initial geometric imperfections nor residual stresses from welding flange and web plates significantly influence cyclic behaviour beyond the first half-cycle. To verify this, a residual stress distribution proposed by Susantha *et al.* (2005) was selected and applied to the pier, as shown in Figure 7. A similar distribution was also recommended by Yao & Fujikubo (2016) for T-sections.

The proposed model for the residual stress distribution accurately represents its effects on the pier, providing the necessary details for precise stress modeling and calculation. The residual stress is applied in the axial direction following specified values, ensuring a realistic representation in the numerical model. Figure 8 illustrates the applied stress distribution, which is also incorporated into the steel plate, stiffeners, and diaphragms.

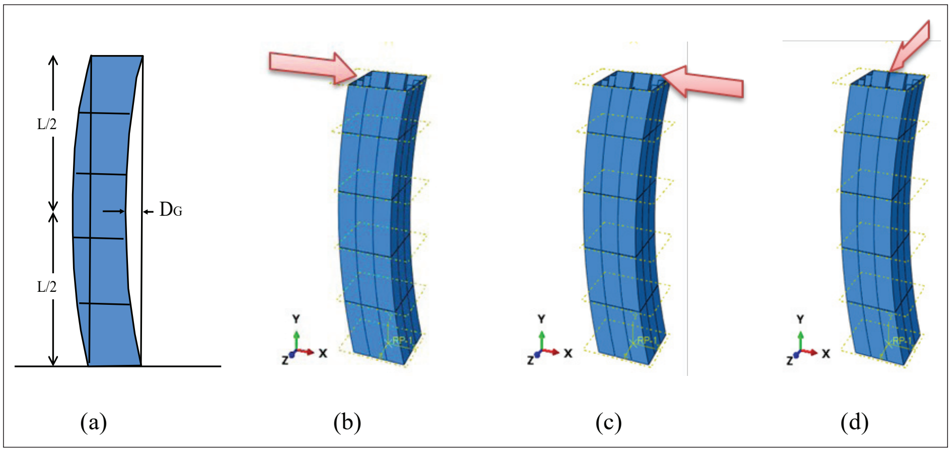

Figure 9: Global geometric imperfection modeling: (a) indication of the curved profile, (b) unidirectional cyclic loading applied in +X-direction and (c) unidirectional cyclic loading applied in -X-direction (d) unidirectional cyclic loading applied in Z-direction

Table 2: Profiles of global geometric imperfections (Permissible range: $D_G \leq L/1500$)

Profile	Initial central deflection (D_G)	Loading Direction
GI 1	$2141 \times \frac{3/3}{1500} = 1.427$ mm	X - Direction
GI 2	$2141 \times \frac{2/3}{1500} = 0.951$ mm	
GI 3	$2141 \times \frac{1/3}{1500} = 0.476$ mm	
GI 4	$2141 \times \frac{3/3}{1500} = 1.427$ mm	Z - Direction
GI 5	$2141 \times \frac{2/3}{1500} = 0.951$ mm	
GI 6	$2141 \times \frac{1/3}{1500} = 0.476$ mm	

Numerical model with global geometric imperfections

The global geometric imperfection taken into account is a bend in the steel pier, as suggested by Sato *et al.* (2017). Therefore, the numerical model must integrate this imperfection profile while maintaining the same arrangement of stiffeners and intermediate diaphragms, as illustrated in Figure 9. In the parametric study, a single curved shape profile with varying bend amplitudes was examined to analyze the way it is influenced by unidirectional cyclic loading, as mentioned in Table 2. The study identifies different cases of global geometric imperfections based on the direction of cyclic load application, as depicted in Figure 9 (b), (c) and (d). The exaggerated shapes illustrating these profiles are presented in Figure 9 (a) to provide a clear indication of the curved profile. To further investigate the effect of these bends, a parametric study was conducted using steel piers with the same cross-sectional arrangement.

Table 3: The selected values for the parametric study

Width to thickness ratio - R_f	Slenderness ratio - λ	Applied axial load to yield load ratio - P/Py
0.5	0.3	0.15
0.6	0.4	
0.7	0.5	0.20
0.8	0.6	

The selected values for the parametric study are provided in Tables 2 and 3. The bend shapes are selected within a range of 0 mm to 70 mm, both within and outside the permissible range specified by Sato *et al.* (2017), where the permissible deviation for global imperfections was ≤ L/1500. Global geometric imperfections are introduced by modeling the curved shape in ABAQUS software. The results obtained from these simulations are used to determine a fixed curvature for further studies on the sensitivity analysis. The sensitivity analysis was focused on the main design parameters of steel piers, such as width-to-thickness ratio, slenderness ratio, and axial load-to-yield load ratio, while keeping the stiffener properties and loading arrangement constant. Tables 4 and 5 contain the critical data necessary to model the test piers in this sensitivity analysis.

Table 4: Essential values for modeling (P/P_y=0.15)

No	P/P_y	R_f	λ	P(kN)	δ_y	H_y/(kN)
1	0.15	0.50	0.30	905.51	10.75	469.06
2	0.15	0.50	0.40	905.51	18.70	343.61
3	0.15	0.50	0.50	905.51	28.38	266.70
4	0.15	0.50	0.60	905.51	39.30	214.46
5	0.15	0.60	0.30	795.49	10.82	409.93
6	0.15	0.60	0.40	795.49	18.85	300.08
7	0.15	0.60	0.50	795.49	28.55	233.24
8	0.15	0.60	0.60	795.49	39.68	187.13
9	0.15	0.70	0.30	691.05	10.70	353.03
10	0.15	0.70	0.40	691.05	18.50	259.54
11	0.15	0.70	0.50	691.05	28.14	201.18
12	0.15	0.70	0.60	691.05	39.03	161.61
13	0.15	0.80	0.30	606.96	10.42	308.77
14	0.15	0.80	0.40	606.96	18.11	226.35
15	0.15	0.80	0.50	606.96	27.47	175.77
16	0.15	0.80	0.60	606.96	38.12	141.16

Table 5: Essential values for modeling (P/P_y=*0.20*)

No	P/P_y	R_f	λ	P(kN)	δ_y	H_y / (kN)
17	0.20	0.50	0.30	1207.34	10.17	443.78
18	0.20	0.50	0.40	1207.34	17.54	322.30
19	0.20	0.50	0.50	1207.34	26.32	247.32
20	0.20	0.50	0.60	1207.34	35.93	196.03
21	0.20	0.60	0.30	1060.65	10.24	387.84
22	0.20	0.60	0.40	1060.65	17.69	281.48
23	0.20	0.60	0.50	1060.65	26.48	216.31
24	0.20	0.60	0.60	1060.65	36.27	171.04
25	0.20	0.70	0.30	921.40	10.12	333.99
26	0.20	0.70	0.40	921.40	17.35	243.46
27	0.20	0.70	0.50	921.40	26.09	186.56
28	0.20	0.70	0.60	921.40	35.67	147.71
29	0.20	0.80	0.30	809.29	9.86	292.13
30	0.20	0.80	0.40	809.29	16.99	212.32
31	0.20	0.80	0.50	809.29	25.47	163.01
32	0.20	0.80	0.60	809.29	34.84	129.02

RESULTS AND DISCUSSION

Validation of the numerical model

The importance of mesh density in getting accurate results was checked through a mesh sensitivity analysis. Figure 10 shows how different mesh sizes, from 50 mm to 10 mm, affect base shear results. This confirms that refining the mesh is necessary for reliable analysis. Based on this, a 25 mm mesh size was selected for the study.

The loading pattern displayed in Figure 4 was applied to the steel hollow column for model validation, with reference to experimental data from Susantha *et al.* (2007). The envelop curve of the FEM numerical model, shown in Figure 11, demonstrates favourable agreement with the experimental curve.

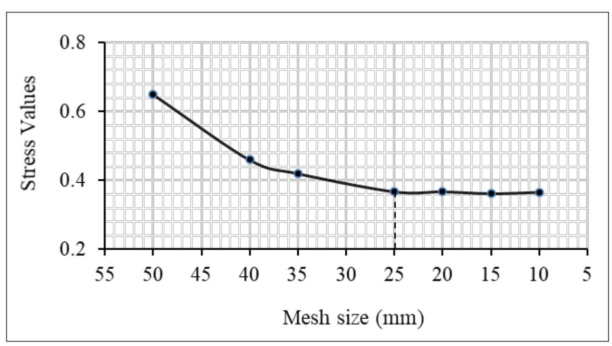

Figure 10: Variation of base stress with size of the mesh

Additionally, the numerical deformation shapes matched precisely with those from the experimental study. Figure 12 illustrates a comparison of the buckling shape at the fixed base observed by Susantha *et al.* (2007) with the buckling shape of the perfect model.

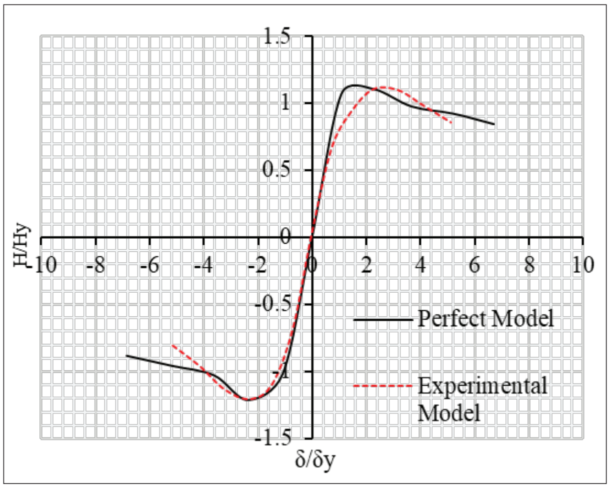

Figure 11: Envelope

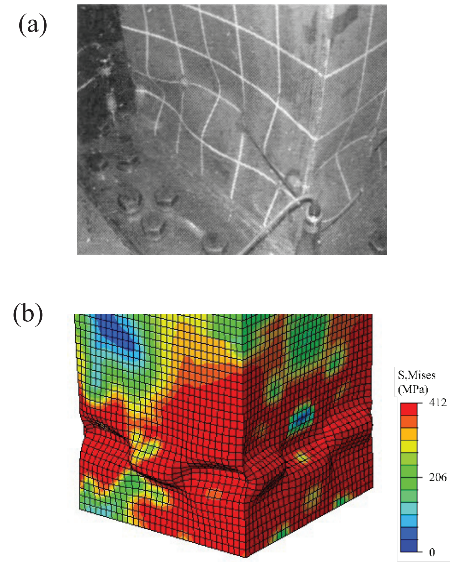

Figure 12: Buckling behaviour: (a) experimental model and (b) numerical model (Susantha *et al.*, 2007)

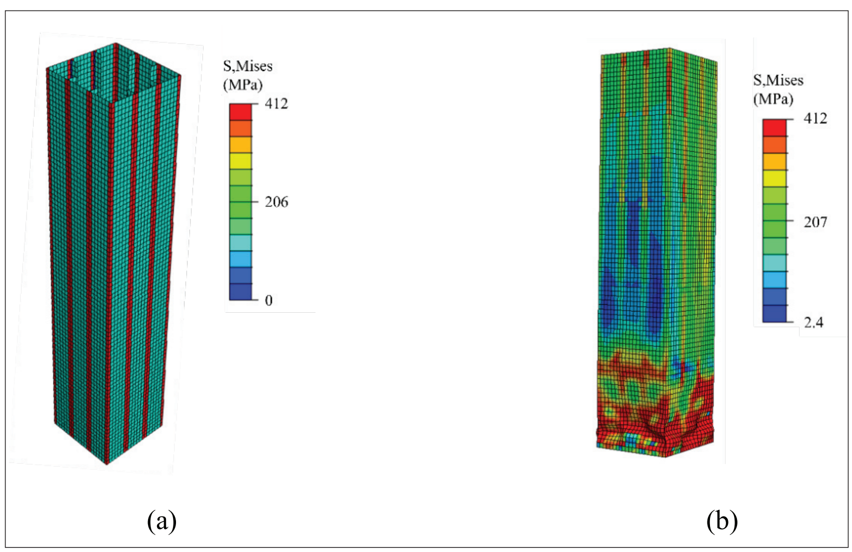

Figure 13: Model with residual stresses: (a) residual stress distribution of the pier and (b) deformed shape and von Mises stresses after failure

Results of residual stress study

In this study, residual stress distribution derived from Susantha *et al.* (2007) was incorporated into the test model, which allowed us to evaluate its impact on the seismic performance of steel hollow piers. A comparison with an idealized model under similar seismic conditions indicated that residual stress has a minimal impact on the seismic behaviour of steel piers. Figure 13(a) provides a visual representation of the stress distribution across the pier following the application of residual stresses, while Figure 13(b) illustrates the deformed shape and corresponding stress values after being subjected to lateral cyclic loading until failure.

Figure 14 presents a comparison between the perfect model (free from any initial imperfections) and the performance of the model with residual stresses, employing the envelop curve. Based on the results, the effect of residual stress on the seismic performance of steel hollow sections is negligible. The numerical analysis and comparison with experimental data indicate that the presence of residual stress does not significantly alter the structural behaviour under seismic loading.

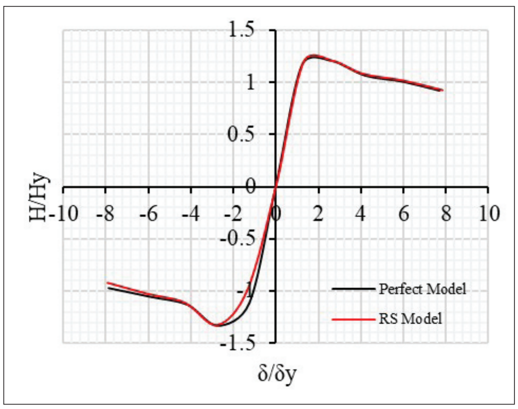

Figure 14: Comparison of the perfect model performance and RS model performance using envelop curve

Results of global geometric imperfections study

This section presents the results of the study on global geometric imperfections. First, the permissible range was checked using the test pier, as described by Sato *et al.* (2017). The results within this range are shown in Figure 15. Since there was no strength reduction within the permissible range, we examined cases beyond this limit (D_G > L/1500), as shown in Figure 16. A significant effect was observed when the bend profile was D_G = L/50. This condition was used for sensitivity analysis to evaluate its impact on R_f, H/H_y, and P/P_y, as presented in Table 3. The analysis was conducted for both X-direction and Z-direction loading conditions.

Tables 6 and 7 present the results for δ_{max}/δ_y of the sensitivity analysis conducted in this study.

Table 6, δ_{max}/δ_y variation with R_f values for P/P_y = 0.15 does not show a consistent trend in δ_{max}/δ_y changes with different R_f values. In most cases, the δ_{max}/δ_y decreases as the λ value increases, although there are instances where it increases significantly. The overall tendency is a decrease in δ_{max}/δ_y with rising λ values, but this variation occurs because δ_{max}/δ_y is influenced by multiple factors related to the cross-sectional parameters. Additionally, with the inclusion of global imperfections, the δ_{max}/δ_y shows variation when compared to the perfect model response. This indicates that δ_{max}/δ_y is indeed influenced by global imperfections. Further studies with possible experimental work should be conducted to identify a trend in variations of these parameters when the models are subjected to global imperfections.

Tables 6 and 7 present the results for δ_{max}/δ_y of the sensitivity analysis conducted in this study.

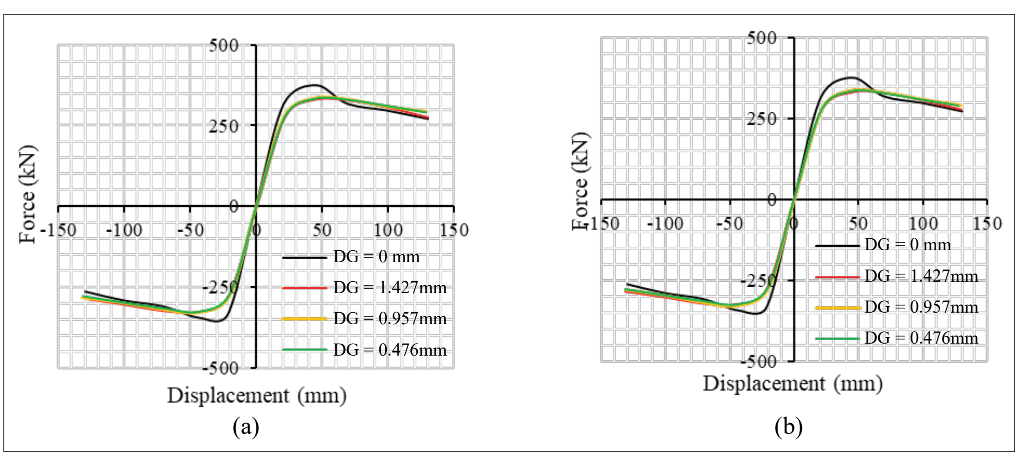

Figure 15: Results on permissible range: (a) X-direction loading and (b) Z-direction loading

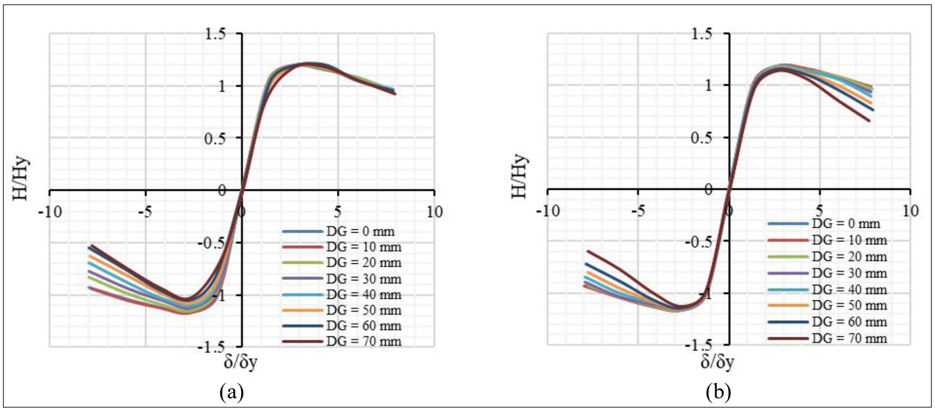

Figure 16: Comparison of results with different D_G values (a) X-direction loading, (b) Z-direction loading

Table 6: δ_{max}/δ_y variation with R_f values for $P/P_y = 0.15$

<table>
<tr><td></td><td>X direction loading</td><td>Z direction loading</td></tr>
<tr><td>+ displacement</td><td>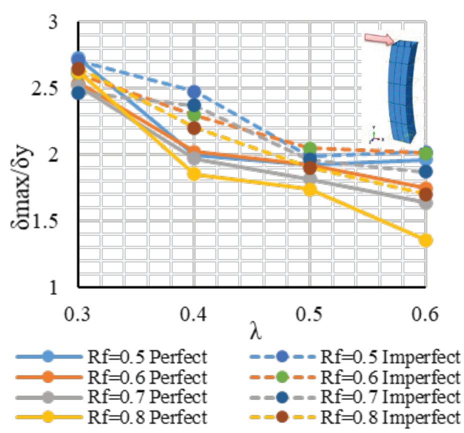
</td><td>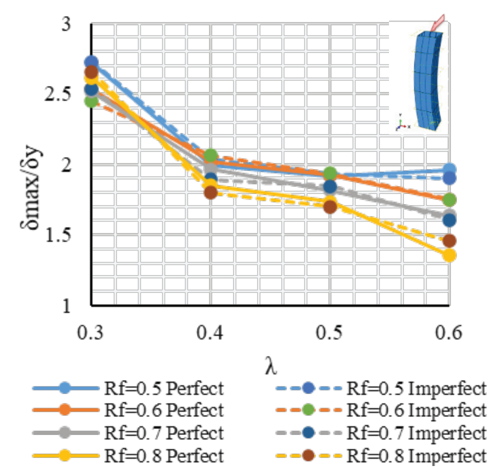
</td></tr>
<tr><td>- displacement</td><td>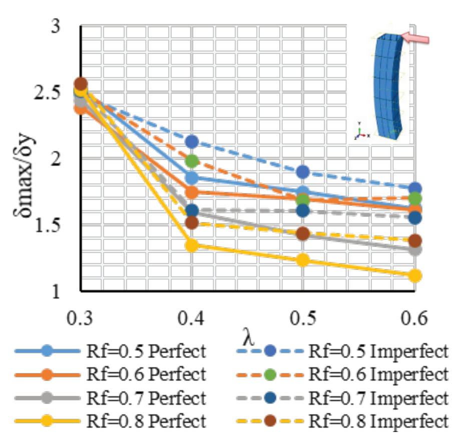
</td><td></td></tr>
</table>

Table 7: δ_{max}/δ_y variation with R_f values for $P/P_y = 0.20$

	X direction loading	Z direction loading
+ displacement	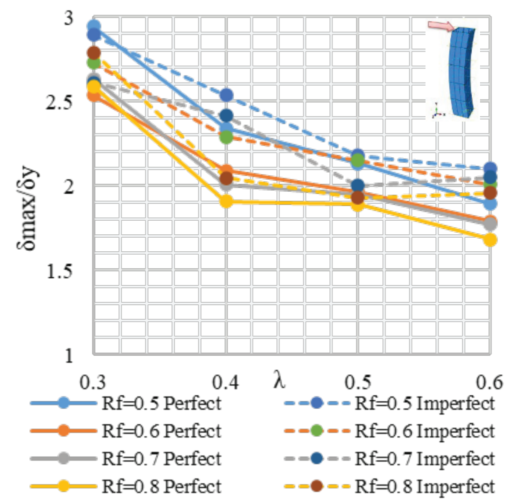	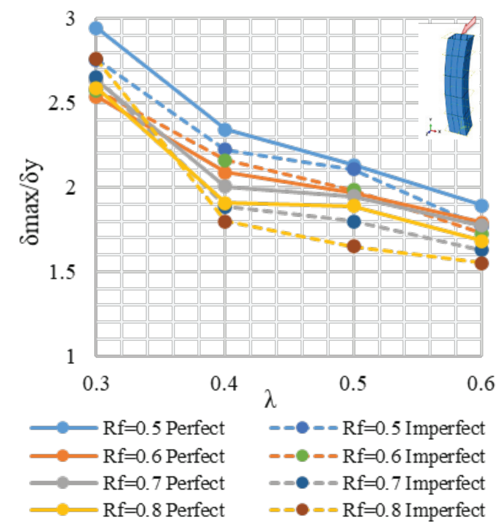
- displacement	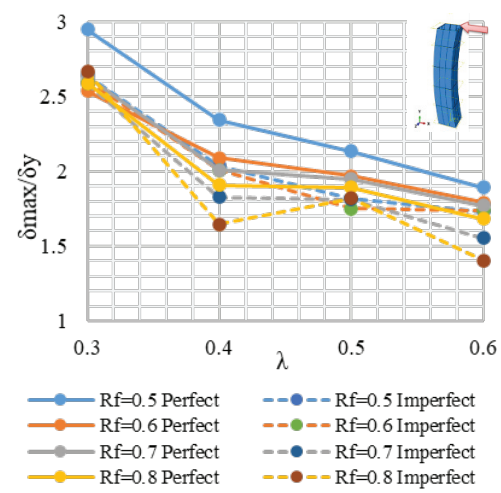	

For the case of P/P_y = 0.20, a clear trend could not be identified from the study either. However, similar to the P/P_y = 0.15 scenario, a reduction in δ_{max}/δ_y with increased λ values was observed, as shown in Table 7.

Tables 8 and 9 present the results for H_{max}/H_y of the sensitivity analysis conducted in this study.

From above percentage reduction values, it can be identified that the +X direction displacement heavily affects the maximum strength of the pier. For the case of R_f = 0.8 and λ = 0.6, there is a 24% reduction in +X direction displacement, but less than 11% in the -X direction. For the Z direction, both negative and positive displacements exhibit similar behaviour due to symmetry, with reductions ranging between 1% and 11%.

Table 8: Percentage reduction of H_{max}/H_y (P/P_y = 0.15)

R_f	λ	H_{max}/H_y +X Perfect	+X Imper-fect	+X % reduction	-X Perfect	-X Imper-fect	-X % reduction	Z Perfect	Z Imper-fect	Z % reduction
0.5	0.3	1.25	1.18	**5.49**	1.25	1.25	**-0.28**	1.25	1.23	**1.20**
	0.4	1.17	1.07	**8.91**	1.17	1.15	**1.77**	1.17	1.13	**4.02**
	0.5	1.14	1.01	**11.09**	1.14	1.12	**1.63**	1.14	1.09	**4.01**
	0.6	1.04	0.93	**10.19**	1.04	1.06	**-2.39**	1.04	0.97	**6.25**
0.6	0.3	1.22	1.13	**7.77**	1.22	1.19	**2.71**	1.22	1.19	**2.98**
	0.4	1.16	1.02	**11.71**	1.16	1.08	**6.53**	1.16	1.10	**4.88**
	0.5	1.12	0.97	**13.41**	1.12	1.08	**3.67**	1.12	1.08	**3.45**
	0.6	1.02	0.88	**13.70**	1.02	1.05	**-2.72**	1.02	0.95	**6.46**
0.7	0.3	1.20	1.10	**8.18**	1.20	1.14	**4.78**	1.20	1.17	**2.07**
	0.4	1.12	0.98	**12.22**	1.12	1.09	**3.15**	1.12	1.06	**5.00**
	0.5	1.09	0.93	**15.20**	1.09	1.05	**3.86**	1.09	1.04	**4.62**
	0.6	1.00	0.81	**18.92**	1.00	0.98	**1.94**	1.00	0.92	**8.38**
0.8	0.3	1.17	1.04	**10.86**	1.19	1.13	**5.39**	1.16	1.08	**7.27**
	0.4	1.10	0.90	**18.60**	1.11	1.07	**3.57**	1.10	1.01	**8.13**
	0.5	1.04	0.86	**17.06**	1.07	1.03	**4.01**	1.03	0.98	**4.85**
	0.6	0.98	0.79	**20.05**	0.97	0.92	**5.37**	1.00	0.90	**10.20**

Table 9: Percentage reduction of H_{max}/H_y (P/P_y = 0.20)

Rf	λ	H_{max}/H_y +X Perfect	+X Imper-fect	+X % reduction	-X Perfect	-X Imper-fect	-X % reduction	Z Perfect	Z Imper-fect	Z % reduction
0.5	0.3	1.28	1.19	**7.62**	1.28	1.28	**0.37**	1.28	1.25	**2.46**
	0.4	1.17	1.07	**8.71**	1.17	1.16	**1.05**	1.17	1.15	**2.12**
	0.5	1.13	1.02	**10.15**	1.13	1.13	**0.08**	1.13	1.10	**2.50**
	0.6	1.07	0.90	**15.34**	1.07	1.06	**0.28**	1.07	1.00	**6.34**
0.6	0.3	1.23	1.13	**7.97**	1.23	1.21	**1.37**	1.23	1.21	**1.55**
	0.4	1.16	1.01	**12.90**	1.16	1.11	**4.90**	1.16	1.11	**4.26**
	0.5	1.11	0.95	**14.64**	1.11	1.02	**8.30**	1.11	1.08	**2.74**
	0.6	1.05	0.84	**19.97**	1.05	1.00	**4.71**	1.05	0.97	**7.76**
0.7	0.3	1.20	1.10	**8.66**	1.20	1.12	**6.99**	1.20	1.18	**2.02**
	0.4	1.13	0.98	**13.10**	1.13	1.07	**5.12**	1.13	1.07	**4.80**
	0.5	1.08	0.88	**18.37**	1.08	1.01	**6.70**	1.08	1.05	**2.95**
	0.6	1.04	0.78	**24.97**	1.04	0.97	**6.64**	1.04	0.93	**10.46**
0.8	0.3	1.17	0.99	**15.95**	1.17	1.04	**11.09**	1.17	1.10	**6.24**
	0.4	1.09	0.95	**12.85**	1.09	0.99	**8.81**	1.09	1.01	**6.99**
	0.5	1.04	0.87	**15.73**	1.04	0.99	**4.60**	1.04	0.95	**8.14**
	0.6	1.00	0.76	**24.00**	1.00	0.94	**6.06**	1.00	0.89	**10.79**

CONCLUSION

This section summarizes the key findings on how residual stress and global geometric imperfections impact the seismic performance of steel hollow piers. The conclusions are drawn from parametric studies, highlighting the effects of global imperfections, especially residual stresses, on the overall behaviour of piers under seismic loading. These findings provide valuable insights into the role of global imperfections and lay the groundwork for future studies on the combined effects of multiple imperfections.

- The results indicate that residual stress minimally impacts the seismic performance of steel hollow piers. Comparisons with the perfect model reveal negligible differences in ductility and maximum strength, suggesting that residual stress does not significantly influence failure modes or overall seismic behaviour, and its effect is relatively minor in this context.

- Global geometric imperfections have a significant impact on the seismic performance of steel hollow piers when they exceed the permissible range (D_G > L/1500). The effect becomes more pronounced as P/P_y and λ values increase, indicating a strong correlation between these parameters and the reduction in ductility and strength (up to 24%) which emphasizes the significance of considering the effect of global imperfections in steel box piers in the design stages. Additionally, the direction of loading relative to the imperfection shape plays a critical role, with loading towards the bend causing a more significant reduction in performance compared to other directions.

- The direction of loading relative to the imperfection profile notably affects seismic behaviour. Loading in the +X direction results in a more pronounced reduction in performance compared to the -X direction. In the Z direction, although the behaviour is not perfectly symmetrical, the observed differences are minor.

REFERENCES

Alpsten, G.A., & Tall, L., 1970. *Residual stresses in heavy welded shapes* (pp. 93-105). American Welding Society.

Aoki, T., & Susantha, K.A.S. (2005). Seismic Performance of Rectangular-Shaped Steel Piers under Cyclic Loading. *Journal of Structural Engineering*, 131(2), pp.240–249. doi:https://doi.org/10.1061/(asce)0733-9445(2005)131:2(240)

Bambach, M.R., & Rasmussen, K.J.R., 2001, June. Residual stresses in unstiffened plate specimens. In *Third International Conference on Thin-Walled Structures, Cracow, Poland* (pp. 87-93).

Bjorhovde, R., Brozzetti, J., Alpsten, G.A., & Tall, L., 1972. Residual stresses in thick welded plates. *WELD J--MIAMI FLA--*, *51*(8), p.292.

British Standards Institution (2022). *BS EN 1993-1-5. Eurocode 3. Design of Steel Structures*.

Cao, X., Xu, Y., Kong, Z., Shen, H., & Zhong, W., 2017. Residual stress of 800MPa high strength steel welded T section: Experimental study. *Journal of Constructional Steel Research*, 131, pp.30–37. https://doi.org/10.1016/j.jcsr.2016.12.001.

Chen, B.-Q., & C. Guedes Soares (2021). Experimental and numerical investigation on welding simulation of long stiffened steel plate specimen. *Marine Structures*, 75, pp.102824–102824. https://doi.org/10.1016/j.marstruc.2020.102824.

Chen, S., Xie, X., & Hanqing Zhuge (2019). Hysteretic model for steel piers considering the local buckling of steel plates. Engineering Structures, 183, pp.303–318. https://doi.org/10.1016/j.engstruct.2018.12.101.

Clarin, M., 2003. Measurement of longitudinal residual stresses in a cold formed rectangular hollow section. *Structural Design of Cold Worked Austenitic Stainless Steel, Internal Rep*, pp.08-30.

Clarin, M., 2004. *High strength steel: local buckling and residual stresses* (Doctoral dissertation, Luleå tekniska universitet).

Dang, J., Yuan, H., Igarashi, A., & Aoki, T. (2017). Multiple-Spring Model for Square-Section Steel Bridge Columns under Bidirectional Seismic Load. *Journal of Structural Engineering*, 143(5), p.04017005. https://doi.org/10.1061/(asce)st.1943-541x.0001735.

Dwight, J.B., Chin, T.K., & Ractliffe, A.T., 1968. Local buckling of thin-walled columns, effect of locked-in welding stresses. *CIRIA, Res. Rep. No. 12, May 1968*.

Fujie, W., Taguchi, M., Kang, L., Ge, H., & Xu, B., 2020. Ductile crack initiation evaluation in stiffened steel bridge piers under cyclic loading. *Steel and Composite Structures*, *36*, pp.463-480.

Goto, Y., Jiang, K., & Obata, M. (2006). Stability and Ductility of Thin-Walled Circular Steel Columns under Cyclic Bidirectional Loading. *Journal of Structural Engineering-asce*, 132(10), pp.1621–1631. https://doi.org/10.1061/(asce)0733-9445(2006)132:10(1621).

Haffar, M.Z., Kövesdi, B., & Adany, S. (2021). Buckling of compressed plates with closed-section longitudinal stiffeners: Two new mathematical models for resistance prediction. *Structures*, 33, pp.3526–3539. https://doi.org/10.1016/j.istruc.2021.06.083.

Hassan, M.S., Salawdeh, S., & Goggins, J. (2018). Determination of geometrical imperfection models in finite element analysis of structural steel hollow sections under cyclic axial loading. *Journal of Constructional Steel Research*, 141, pp.189–203. https://doi.org/10.1016/j.jcsr.2017.11.012.

Hsu, H., & Juang, J.-L. (2000). Performance of thin-walled box columns strengthened with internal braces. *Thin-Walled*

Structures, 37(3), pp.241–258. https://doi.org/10.1016/s0263-8231(00)00020-3.

Ingvarsson, L., 1977. *Cold-forming residual stresses and box columns built up by two cold-formed channel sections welded together*. Department of Structural Mechanics and Engineering, Royal Institute of Technology.

Jenothan, M., Jayasinghe, J.A.S.C., & Bandara, C.S. (2023). Lateral behaviour and performance evaluation of steel piers under cyclic lateral loading. *Journal of Constructional Steel Research*, 201, p.107764. https: //doi.org/10.1016/j.jcsr.2022.107764

Jenothan, M., Jayasinghe, C., Bandara, C.S., & Dammika, A.J. (2024). Performance evaluation of steel hollow box piers under bidirectional lateral cyclic loading to enhance the existing seismic verification framework. *Journal of Constructional Steel Research*, 212, pp.108246–108246. https://doi.org/10.1016/j.jcsr.2023.108246

Jenothan, M., Jayasinghe, C., Bandara, C.S., & Dammika, A.J. (2023). Thin-Walled Hollow Steel Box Piers with Energy Dissipation Mechanism Under Bi-directional Cyclic Loading. *Lecture Notes in Civil Engineering*, pp.29–45. doi:https: //doi.org/10.1007/978-981-99-3471-3_3

Jiang, H., Hu, X., Wang, T., & Sun, Z., 2021, July. Experimental and numerical study on thin-walled hollow bridge piers. In *IOP Conference Series: Earth and Environmental Science* (Vol. 820, No. 1, p. 012004). IOP Publishing.

Kollár, D., Völgyi, I., & Joó, A.L. (2023). Assessment of residual stresses in welded T-joints using contour method. *Thin-Walled Structures*, 190, pp.110966–110966. https://doi.org/10.1016/j.tws.2023.110966.

Kövesdi, B., Haffar, M.Z., & Ádány, S. (2021). Buckling resistance of longitudinally stiffened plates: Eurocode-based design for column-like and interactive behavior of plates with closed-section stiffeners. *Thin-Walled Structures*, 159, p.107266. https://doi.org/10.1016/j.tws.2020.107266.

Lagerqvist, O., & Olsson, A., 2001. Residual stresses in welded l-girders made of stainless steel and structural steel. In *Nordic Steel Construction Conference: 18/06/2001-20/06/2001*. Helsinki University of Technology.

Mamaghani, I.H.P. (2008). Seismic Design and Ductility Evaluation of Thin-Walled Steel Bridge Piers of Box Sections. *Transportation Research Record: Journal of the Transportation Research Board*, 2050(1), pp.137–142. https://doi.org/10.3141/2050-14

Nishino, F., Ueda, Y., & Tall, L. (1967). "Experimental Investigation of the Buckling of Plates with Residual Stresses", ASTM Special Technical Publication, No. 419. pp. 12-30

Rossini, N.S., Dassisti, M., Benyounis, K.Y., & Olabi, A.G. (2012). Methods of measuring residual stresses in components. *Materials and Design*, 35, pp.572–588. https://doi.org/10.1016/j.matdes.2011.08.022

Sato, A., Mitsui, K., Aoyama, M., & Inden, A. K. (2017). Effect of initial imperfection on elasto-plastic behavior of square steel tubular columns under compressive axial force with monotonic antisymmetric bending moment. *Journal of Structural and Construction Engineering*, *82*(741), 1787-1797. https://doi.org/10.3130/aijs.82.1787

Shen, Z., & Zhang, Q. (1991). Interaction of Local and Overall Instability of Compressed Box Columns. *Journal of Structural Engineering-ASCE*, 117(11), pp.3337–3355. doi:https://doi.org/10.1061/(asce)0733-9445(1991)117:11(333)

Shi, G., Zhou, W., Bai, Y., & Lin, C. (2014). Local buckling of 460MPa high strength steel welded section stub columns under axial compression. *Journal of Constructional Steel Research*, 100, pp.60–70. https://doi.org/10.1016/j.jcsr.2014.04.027

Smith, D.J., & Bonner, N.W. (1996). "Measurement of Residual Stresses Using the Deep Hole Method", PVP-Vol. 327, Residual Stresses in Design Fabrication, Assessment and Repair, ASME, 1996.

Susantha, K.A.S., Aoki, T., & Jayasinghe, M.T.R. (2007). Finite Element Analysis of Steel Columns Subjected to Bi-directional Cyclic Loads. *Engineer: Journal of the Institution of Engineers, Sri Lanka*, 40(4), p.35. https://doi.org/10.4038/engineer.v40i4.7152

T. Thevega, K. Rajavijayan, Jayasinghe, C., & K.A.S. Susantha (2021). Strength and Ductility of Stiffened Steel Box Columns of Various Cross-Sectional Configurations under Lateral Cyclic Loadings. 54(2), pp.25–25. https://doi.org/10.4038/engineer.v54i2.7440

Usami, T., & Ge, H.B. (1998). Cyclic behaviour of thin-walled steel structures—numerical analysis. *Thin-Walled Structures*, 32(1-3), pp.41–80. https://doi.org/10.1016/s0263-8231(98)00027-5

Walker, D., 2001. Residual stress measurement techniques. *Advanced Materials & Processes*, *159*(8), pp.30–30.

Watanabe, E., Sugiura, K., & Oyawa, W.O., 2000. Effects of multi-directional displacement paths on the cyclic behaviour of rectangular hollow steel columns. *Doboku Gakkai Ronbunshu*, *2000*(647), pp.79–95. https://doi.org/10.2208/jscej.2000.647_79

Watanabe, E., Sugiura, K., Nagata, K., & Kitane, Y. (1998). Performances and damages to steel structures during the 1995 Hyogoken-Nanbu earthquake. *Engineering Structures*, 20(4-6), pp.282–290. https://doi.org/10.1016/s0141-0296(97)00029-1

Weisman, C., & Kearns, W.H. *eds.*, 1976. *Welding Handbook: Metals and their weldability* (Vol. 4). American Welding Society.